ELSEVIER

International Journal of Heat and Fluid Flow 19 (1998) 39–48

International Journal of HEAT AND FLUID FLOW

Effect of Tollmien Schlichting wave on convective heat transfer in a wavy channel. Part I: Linear analysis

S. Blancher [a,*], R. Creff [a], P. Le Quere [b]

[a] *Laboratoire de Transferts Thermiques, Hèlioparc Avenue du Président Angot, 64000 Pau, France*
[b] *LIMSI CNRS, BP 139, 91403 Orsay Cedex, France*

Received 1 February 1997; accepted 20 August 1997

Abstract

Hydrodynamic instabilities in wavy channels and their effect on the convective heat transfer are investigated using both linear stability analysis and integration of the time dependent Navier–Stokes and energy equations. The linear stability of the fully developed flow is determined from a generalized eigenvalue problem resulting from a Galerkin approach using divergence free Chebychev basis functions and trigonometric polynomials. Several axial periodicity lengths to geometry length ratios have been considered. For our geometry, the instability is found to set in as a Tollmien Schlichting wave, at a Reynolds number approximately equal to 90. The dynamics of the detachment and reattachment points and of temperature field for constant wall temperature are examined under the assumption of small amplitude fluctuations. It is shown that, although the average heat transfer remains almost constant, large amplitude variations of the local heat transfer coefficient can be observed, this effect is increasing with increasing Prandtl number.

Notation

Dimensional symbols

E	geometrical amplitude of the wall shape (m)
H_0	minimum half height of the channel (m)
L	spatial period of the channel (m)
T	temperature (°C)
U_0	average mean velocity (m/s)

Dimensionless symbols

C_f	wall shear stress coefficient
h	shape of the wall
i	complex number ($i^2 = -1$)
M	number of geometrical periodicity length
Nu	Nusselt number
P_j, Q_m	Polynomials
Pe	Peclet number
Pr	Prandtl number
Re	Reynolds number
t	time
(u, v)	velocity components
(x, y)	cartesian co-ordinates

Greek

Δ, Δ', Δ'', Δ_h	Laplacians
$\zeta = \sigma + i\gamma$	eigenvalues
(ξ,η)	co-ordinates
λ	reduced half period $= (L/H_0)/\pi$
ψ	stream function
ω	vorticity
θ	temperature
φ	heat flux density

Symbols

$(\ )'$; $(\ )''$	ξ derivative
$(\ )_\xi$	partial ξ derivative
$(\ )_\eta$	partial η derivative
$(\ )_t$	partial time derivative
$(\ )^0$	steady solution
$(\ )^1$	perturbation
$(\ )^S$	straight channel
Re	real part
Im	imaginary part

1. Introduction

Flows in converging–diverging periodic channels are present in numerous applications such as compact heat transfer exchangers, blood oxygenators, cooling of microelectronics components. They have been studied intensively over the last 20 years. The first numerical studies were performed by Sobey (1980), who solved the two-dimensional Navier–Stokes equations by a finite difference method, assuming a sinusoidal pulsed flow rate modulation. The experimental visualisations by Stephanoff et al. (1980) later confirmed Sobey's results. Asako and Faghri (1987) have made a numerical simulation for a steady laminar flow by a finite volume approach.

* Corresponding author. E-mail: serge.blancher@univ-pau.fr.

0142-727X/98/$19.00
PII: S0142-727X(97)10009-1

Nishimura et al. (1983, 1985) performed some experiments on the mass transfer characteristics using an electrochemical technique for the steady laminar flow. These experiments were carried out in parallel with numerical simulations by a finite element method and flow visualizations for steady (Nishimura et al., 1990) and transitional flows (Nishimura et al., 1986). Simultaneously, we investigated the steady laminar dynamic and thermal flow fields (Blancher, 1991) – in these particular geometries by numerical simulations using a Galerkin spectral method (Canuto et al., 1988). Ellouze (1993) made a direct two-dimensional simulation of the non-linear equations using a finite difference discretization. The general conclusions of these studies is that beyond a critical Reynolds number, the flow becomes unsteady and is then characterised by the presence of symmetric transverse vortices. This then leads to a decrease of the average heat transfer in comparison with the straight channel, taking into account the pressure drop penalty. However large local heat transfer enhancement (up to 80%) can be obtained locally – in the case of constant temperature boundary condition only. This enhancement is localised slightly upstream the minimum section, just after the reattachment point, corresponding to the boundary layer redevelopment. As shown by Asako and Faghri (1987), average heat transfer enhancement can also be obtained beyond a critical Reynolds number for high Prandtl number fluids.

In addition, flow visualisations by Nishimura et al. (1983, 1985) have shown that the onset of unsteadiness occurs for a critical Reynolds number approximately equal to 100, which is much smaller than in a straight channel O(1000). The experiments performed by Stephanoff (1980) have shown that the self-excited shear layer oscillations appear at one or sometimes two selectively amplified frequencies. A linear stability analysis as described by Drazin and Reid (1981) allowed us to obtain the critical Reynolds number and the nature of these instabilities. This study showed that the first instability (the most dangerous mode) is a Tollmien Schlichting (TS) wave with a wavelength and frequency which depend on the geometry. Some hot wire anemometer measurements (Blancher, 1991; Blancher et al., 1992) have also been made. These results have confirmed the critical Reynolds number and the fundamental frequencies which were obtained numerically. Slightly beyond this critical Reynolds number the flow is periodic in time. Similar behaviour was observed by Ghaddar et al. (1986) or Greiner et al. (1990) in grooved periodic geometries, who called it "self sustained oscillating flow". It can thus be stated that the sustained time periodic nature of the flow is due to the periodic variations of the channel cross section. More recently a direct three-dimensional numerical simulation by Guzman and Amon (1993) using a spectral element method has confirmed that the first instability mechanism in the geometry considered in the experiments by Nishimura et al. (1983) is indeed a two-dimensional TS wave. Increasing the Reynolds number, quasi-periodicity appears and thereafter chaos follows. The authors have proposed a "route to turbulence" corresponding to the Ruelle Takens scenario.

In this paper we propose to analyse the mechanism of the local heat transfer enhancement due to the TS wave perturbation. More precisely, we want to address the important issue of the heat transfer enhancement beyond onset of unsteadiness in the linear approximation, i.e. in the limit of infinitesimal disturbances. The non-linear effects will be addressed elsewhere. We first recall the numerical methodology based on a spectral Galerkin method, which allows us to obtain the dynamic and thermal characteristics of a steady laminar fully developed flow. The linear stability of this flow is then investigated under the assumption of two-dimensional infinitesimal perturbation. This stability analysis gives the critical Reynolds number beyond which the flow bifurcates to an unsteady one and the dynamic characteristics of the corresponding eigenmode, which takes the form of a TS wave. The influence of the ratio of the periodicity to geometry length in the axial direction is investigated. The dynamic results are analysed through the velocities and vorticity amplitude fluctuations and the unsteady wall shear stress coefficients $C_f(x,t)$. This dynamic perturbation is then introduced in the energy equation and after linearization the temperature perturbation associated with the TS wave is obtained by a spectral method in the case of uniform and constant wall temperature. The temperature fluctuations, the wall heat flux density fluctuations, the unsteady temperature isotherms and the time averaged local Nusselt number are presented. Finally we discuss the influence of the amplitude for the TS perturbation on the heat transfer enhancement.

2. Problem definition and governing equations

2.1. Geometrical configuration

We consider a diverging–converging symmetric two-dimensional (x, y) channel. The shape of the upper wall profile is $y = h(x)$. We suppose that the function h is periodic along the x axis and twice differentiable. We assume the flow to be laminar, incompressible, unsteady, two-dimensional and periodically fully developed. The fluid is homogeneous, viscous with constant uniform physical properties. Effect of gravity, radiation and natural convection are supposed to be negligible. The hypothesis of fully developed flow results in a velocity or stream function $\psi(x, y, t)$ which are periodic in the direction of the flow (Ox) with a period equal to a multiple (M) of the geometric period $2L$.

2.2. Governing equations

The two-dimensional unsteady Navier–Stokes equations written with the stream function ψ and vorticity ω functions are made dimensionless by scaling lengths by H_0, the minimum half width of the channel, and velocities by $\overline{U}_0$, the averaged velocity at this minimum section. Then the Reynolds number is

$$\mathrm{Re} = \frac{\overline{U}_0 H_0}{\nu}. \tag{1}$$

We define new co-ordinates (ξ, η) by the transformation

$$\xi = x/\lambda \quad \text{and} \quad \eta = y/h(\xi) \tag{2}$$

with $\lambda = (L/H_0)/\pi$. With this transformation, the unsteady Navier–Stokes equations can be written as

$$\tilde{\omega} = -\lambda^2 h^2 \omega = \Delta' \psi, \tag{3a}$$

$$\lambda h^2 \tilde{\omega}_t + h(\psi_\eta \tilde{\omega}_\xi - \psi_\xi \tilde{\omega}_\eta) - 2h'\psi_\eta \tilde{\omega} = \frac{1}{\lambda\,\mathrm{Re}} \Delta'' \tilde{\omega} \tag{3b}$$

and the computational domain becomes the rectangle

$$0 \leqslant \xi \leqslant 2M\pi; \quad -1 \leqslant \eta \leqslant +1. \tag{4}$$

The steady problem was first solved by a spectral Galerkin method (Blancher, 1991). The linear stability of these steady solutions was then investigated. The assumption of small perturbations allows us to look for the stream function as

$$\psi(\xi, \eta, t) = \psi^0(\xi, \eta) + \varepsilon \psi^1(\xi, \eta, t). \tag{5}$$

where ψ^0 is the solution of the steady problem and ψ^1 the unknown perturbation with small amplitude ε. The boundary conditions on the perturbation are

$$\begin{array}{ll} \text{periodicity} & \psi^1(\xi + 2M\pi, \eta, t) = \psi^1(\xi, \eta, t), \\ \text{symmetry} & \psi^1_\eta(\xi, 0, t) = \psi^1_\xi(\xi, 0, t) = 0. \\ \text{flow rate condition} & \psi^1(\xi, \pm 1, t) = 0. \end{array} \quad (6)$$

2.3. The numerical method

The assumption of a fully developed flow and the homogeneous boundary conditions allow us to solve this problem by a spectral Galerkin method. The streamfunction is developed on a basis of trial functions which are tensor products of trigonometric polynomials in ξ by divergence free Chebychev polynomials $P_j(\eta)$ which satisfy homogeneous Dirichlet and Neumann boundary conditions. An explicit formula for $P_1(\eta)$ is $T_{j-6} - 3T_{j-4} + 3T_{j-2} - T_j$ $(j > 6)$. The unknown streamfunction fluctuation is thus expanded as

$$\psi^1(\xi, \eta, t) = \sum_{n=-Nx}^{Nx} \sum_{j=0}^{Ny} \hat{\psi}^1_{n,j}(t) P_j(\eta) \exp(in\xi). \quad (7)$$

Let $\underline{\mathbf{X}}(t)$ be the vector composed by the unknown complex coefficients $\hat{\psi}^1_{n,j}(t)$ and $\underline{\mathbf{Y}}(t)$ the vorticity coefficients $\hat{\omega}^1_{n,j}$. Projection of Eqs. (3a) and (3b) on the trial functions results in the linear system:

$$\underline{\mathbf{Y}} = \underline{\underline{\mathbf{D}}}'\underline{\mathbf{X}}, \quad (8a)$$

$$\underline{\underline{\mathbf{D}}}_t \frac{d\underline{\mathbf{Y}}}{dt} = \underline{\underline{\mathbf{L}}}'\underline{\mathbf{Y}} + \underline{\underline{\mathbf{L}}}\underline{\mathbf{X}} + \frac{1}{\lambda\,\mathrm{Re}}\underline{\underline{\mathbf{D}}}''\underline{\mathbf{Y}}, \quad (8b)$$

where $\mathbf{D}$, $\mathbf{D}_t$, $\mathbf{L}$, $\mathbf{L}'$, $\mathbf{D}''$ are the discrete linear operators defined from Eqs. (3a) and (3b). This coupled system of linear equations with constant coefficients admits solutions of the form $\underline{\mathbf{X}} = \mathrm{Real}\,(\hat{\underline{\mathbf{X}}} \exp(\hat{\zeta}t))$, where $\hat{\zeta}$ is solution of the generalized eigenvalue problem

$$\hat{\zeta}\underline{\underline{\mathbf{A}}}\hat{\underline{\mathbf{X}}} = \underline{\underline{\mathbf{B}}}\hat{\underline{\mathbf{X}}}. \quad (9)$$

The eigenvalue spectrum is classified according to the real part σ of the eigenvalues. Each eigenvalue is associated with an eigenvector which gives the spatial structure of the corresponding perturbation. Note that the symmetry of the geometry will give either symmetric or anti-symmetric modes and that the spectrum is composed of real or complex conjugate pairs. When the imaginary part of the eigenvalue is different from zero, the eigenmode is periodic in time, whereas if it is equal to zero, the eigenmode is steady. Let $\hat{\zeta}_0 = \sigma_0 + i\gamma_0$ be the eigenvalue of maximum real part associated with the eigenvector $\underline{\mathbf{X}}_0$, which is called the most unstable or "dangerous" mode. The linear stability analysis thus gives the critical Reynolds number – beyond which small perturbations are amplified – and the spatial structure of the perturbation at this Reynolds number.

3. Dynamic results

3.1. Introduction

Results have been obtained for symmetric and periodic sinusoidal geometries defined by the shape of the upper wall as: $h(x)/H_0 = 1 + E/H_0 - (E/H_0)\cos(\pi x/L)$, where E is half the amplitude of the wavy channel and H_0 half the width of the channel.

Except if not explicitly stated, all the results presented correspond to:

- Nishimura's geometry (Nishimura et al., 1983), $H_0 = 1.5$ mm; period $2L = 14$ mm $(2L/H_0 = 9.33)$ and amplitude $E = 3.5$ mm $(2E/H_0 = 2.33)$.
- Orders of development $Nx = 8$ and $Ny = 32$.
- A periodicity index M equal to 1.

3.2. Steady flow

Fig. 1 presents the steady streamlines obtained for a Reynolds number of 100. Like in previous numerical simulations and flow visualisations we observe that the steady flow is symmetric and that transverse vortices fill all the top and bottom symmetric furrows. The main stream is almost parallel and the detachment and reattachment points are, respectively, localized at $x/(2L) = 0.103$ and $x/(2L) = 0.837$. Table 1 gives the positions of the detachment and reattachment points for different Nx. Other steady results such as velocity, vorticity and have been presented in previous works.

3.3. Linear stability

3.3.1. Plane channel

The plane two-dimensional channel is a particular case of a wavy channel of zero amplitude. Results obtained by Orszag (1971) can serve to validate the present numerical algorithm. The present algorithm gives a critical Reynolds number of 3848 – with our definitions – corresponding to the classical value of 5772 when the Reynolds number is based on the axis velocity. The corresponding wavelength and frequency are $\alpha = \pi H_0/L = 1.02$ and $\gamma = 0.3563$.

3.3.2. Wavy channel

3.3.2.1. Eigenvalue spectrum. Table 2 shows the first eigenvalues for different Reynolds numbers in the case $M = 1$.

It is seen that the real part of the eigenvalues increases with the Reynolds number. In particular, the eigenvalue $\hat{\zeta}_0$ corresponding to the most unstable mode (mode "0") has a real part which becomes positive for a Reynolds number between 80 and 100. We can thus conclude that the critical Reynolds number for linear instability lies between these two values. The corresponding non-zero imaginary part indicates a Hopf bifurcation. It is noted that, in the time unit considered here, the dimensionless frequency of a given mode depends very little on the Reynolds number. The associated dimensional frequencies are defined as follows,

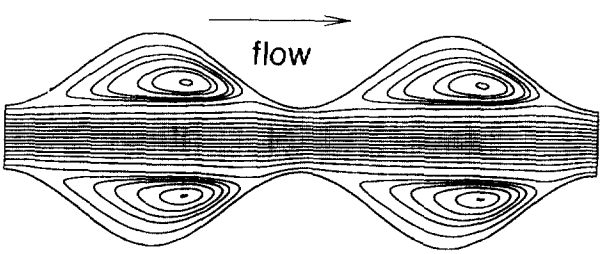

Fig. 1. Nishimura geometry – steady streamlines (Re = 100).

Table 1

	$Nx = 4$	$Nx = 6$	$Nx = 8$	$Nx = 10$	$Nx = 12$	$Nx = 16$
$X_d/(2L)$	0.10218	0.10234	0.10321	0.10349	0.10351	0.10334
$X_r/(2L)$	0.83646	0.83769	0.83739	0.83744	0.83744	0.83731

Table 2

	Re = 60	Re = 80	Re = 100	Re = 120
ζ_0	$-0.3015 \times 10^{-1} \pm$ i 0.24110	$-0.7762 \times 10^{-2} \pm$ i 0.24474	$+0.8443 \times 10^{-2} \pm$ i 0.24761	$+0.3334 \times 10^{-1} \pm$ i 0.76968
ζ_1	$-0.8821 \times 10^{-1} \pm$ i 0.78522	$-0.3579 \times 10^{-1} \pm$ i 0.77695	$+0.3040 \times 10^{-2} \pm$ i 0.77257	$+0.2114 \times 10^{-1} \pm$ i 0.24981
ζ_2	$-0.1048 +$ i 0.0	$-0.8385 \times 10^{-1} +$ i 0.0	$-0.7006 \times 10^{-1} +$ i 0.0	$-0.5762 \times 10^{-1} \pm$ i 0.55065
ζ_3	$-0.1437 \pm$ i 0.52406	$-0.10390 \pm$ i 0.53905	$-0.7713 \times 10^{-1} \pm$ i 0.54674	$-0.6027 \times 10^{-1} \pm$ i 0.0

Table 3

	$Nx = 4$	$Nx = 6$	$Nx = 8$	$Nx = 10$	$Nx = 12$
ζ_0	$+0.9979 \times 10^{-2} \pm$ i 0.24410	$+0.8597 \times 10^{-2} \pm$ i 0.24770	$+0.8443 \times 10^{-2} \pm$ i 0.24761	$+0.8431 \times 10^{-2} \pm$ i 0.24761	$+0.8431 \times 10^{-2} \pm$ i 0.24761
ζ_1	$-0.9584 \times 10^{-2} \pm$ i 0.79153	$+0.2481 \times 10^{-2} \pm$ i 0.77241	$+0.3040 \times 10^{-2} \pm$ i 0.77257	$+0.2941 \times 10^{-2} \pm$ i 0.77267	$+0.2935 \times 10^{-2} \pm$ i 0.77268
ζ_2	$-0.7180 \times 10^{-1} +$ i 0.0	$-0.7001 \times 10^{-1} \pm$ i 0.0	$-0.7006 \times 10^{-1} \pm$ i 0.0	$-0.7007 \times 10^{-1} \pm$ i 0.0	$-0.7007 \times 10^{-1} \pm$ i 0.0
ζ_3	$-0.7940 \times 10^{-1} \pm$ i 0.54338	$-0.7679 \times 10^{-1} \pm$ i 0.54957	$-0.7713 \times 10^{-1} \pm$ i 0.54674	$-0.7714 \times 10^{-1} \pm$ i 0.54673	$-0.7714 \times 10^{-1} \pm$ i 0.54673

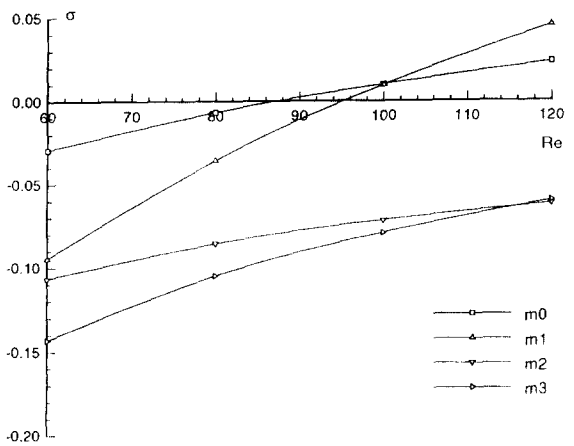

Fig. 2. Real part σ of the eigenvalues ($M = 1$ hypothesis) versus the Reynolds number (critical Reynolds number).

$$f = \frac{\gamma}{2\pi}\frac{\overline{U}_0}{H_0} = \frac{\gamma\,\mathrm{Re}}{2\pi}\frac{\nu}{H_0^2}$$

with $H_0 = 1.5$ mm and $\nu = 1.8 \times 10^{-5}$ m^2/s (air at 20°C) a dimensionless frequency of 0.245 corresponds to a dimensional frequency around 30 Hz.

The real parts σ versus Re are plotted in Fig. 2. The interpolated critical Reynolds number Re_c is approximately 88 for the case $M = 1$. The second most unstable eigenvalue ζ_1 has a real part which becomes positive beyond Re = 95 and the third eigenvalue (mode 2) corresponds to a steady perturbation. Note that the growth rate of mode 1 becomes larger than that of mode 0 for Re > 100.

Influence of the order of development. Table 3 gives the evolution of the first eigenvalues for Re = 100, $M = 1$ as a function of Nx ($Ny = 32$). We can conclude that $Nx = 8$ is large enough to obtain a good approximation of these eigenvalues (real and imaginary parts defined with more than three significative digits).

Table 4

Re	γ_0	γ_0 (Guzman)
83.3	0.2447	0.470235
93.3	0.2452	0.482476
100	0.2476	0.482476
133.3	0.2490	0.482463

Comparison with direct numerical simulation. The above results are in excellent agreement with those obtained by Guzman and Amon (1993) with a direct three-dimensional numerical simulation (in the case $M = 1$). With our Reynolds number definition their critical Reynolds number is between 86.6 and 90. Table 4 compares the reduced frequency γ_0 of the most unstable mode obtained by Guzman and Amon and our results with the hypothesis $M = 1$ (results given with our definitions).

It appears that the values obtained by Guzman are approximately twice the values obtained here. Guzman and Amon determined the frequency from a Fourier analysis of the streamwise velocity component $u(x, 0, t)$ on the symmetry axis. They noted that the fundamental frequencies associated with the x and y directions are in the ratio $\omega_x/\omega_y = 2$. On the symmetry axis, the streamwise velocity eigenfunction is zero, and its instantaneous value thus remains zero in the linear approximation. The frequency doubling of the streamwise velocity $u(x, 0, t)$ comes from the second order non-linear terms neglected in the linear stability analysis, which oscillate at twice the fundamental frequency.

Influence of periodicity hypothesis M. Table 5 presents the first eigenvalues for Re = 100 for different ratios $M = 1$, 2, 3 and 4. To remain numerically consistent Nx was set to $4M$ while Ny was kept equal to 32. This table shows that new unstable modes appear when the geometrical periodicity length M increases, with different fundamental frequencies. The most unstable mode is thus not necessarily the same as in the case $M = 1$, since other modes, not allowed with $M = 1$, can come into play. In our particular case however, the critical Reynolds number remains approximately constant around Re = 90.

Table 5

	$M = 1$	$M = 2$	$M = 3$	$M = 4$
ζ_0	$+0.9979 \times 10^{-2} \pm$ i 0.24410	$+0.2937 \times 10^{-1} \pm$ i 0.49268	$+0.38747 \times 10^{-1} \pm$ i 0.99414	$+0.5544 \times 10^{-1} \pm$ i 0.94692
ζ_1	$-0.9584 \times 10^{-2} \pm$ i 0.79153	$+0.9615 \times 10^{-2} \pm$ i 0.79095	$+0.3062 \times 10^{-1} \pm$ i 0.59311	$+0.2961 \times 10^{-1} \pm$ i 0.49325
ζ_2	$-0.7180 \times 10^{-1} +$ i 0.0	$+0.9336 \times 10^{-2} +$ i 0.24380	$+0.2392 \times 10^{-1} +$ i 0.40230	$-0.2545 \times 10^{-1} \pm$ i 0.62782
ζ_3	$-0.7940 \times 10^{-1} \pm$ i 0.54338	$-0.2414 \times 10^{-2} \pm$ i 1.08369	$+0.2391 \times 10^{-1} \pm$ i 0.26080	$+0.2109 \times 10^{-1} \pm$ i 0.35322

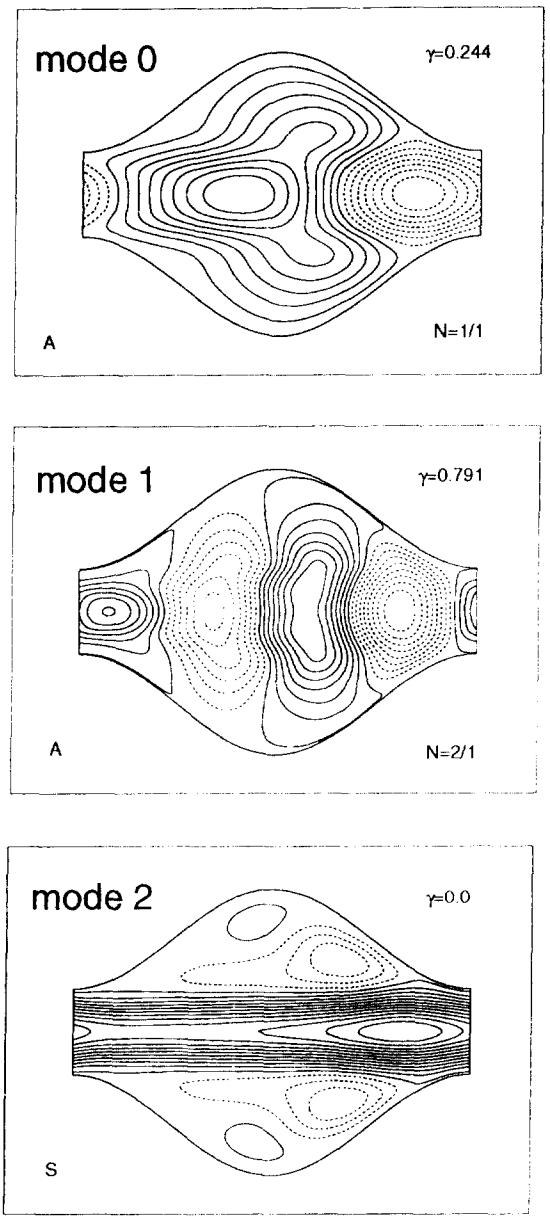

Fig. 3. First eigenmodes ($M = 1$ hypothesis).

3.3.2.2. The Tollmien Schlichting wave. Fig. 3 presents the first three modes in the case $M = 1$. We observe for the most unstable mode (mode 0) a symmetric travelling TS wave, with a wavelength equal to the geometric period $2L$. The second mode (mode 1) has a similar shape but with a wavelength equal to half the geometry length (two TS waves for one geometric period). The next mode is still symmetric but is steady ($\gamma = 0$). The fourth mode (mode 3) is the first anti-symmetric periodic mode, and modes 4 and 5 (not shown) are, respectively, anti-symmetric and symmetric stationary modes.

In the case $M = 2$ the spectrum is made of the modes found for $M = 1$ and of other modes which were not allowed by the $M = 1$ periodicity constraint. In particular the most unstable mode, which has a critical Reynolds number very close to that of the $M = 1$ mode, has a wavelength equal to $\frac{2}{3}$ of the geometric period (three TS waves for two periods). In slightly different geometry we have shown that the wavelength of the unstable mode is not necessarily equal to the spatial geometric period when the periodicity hypothesis is based on $M > 1$ periods of the channel. Other recent

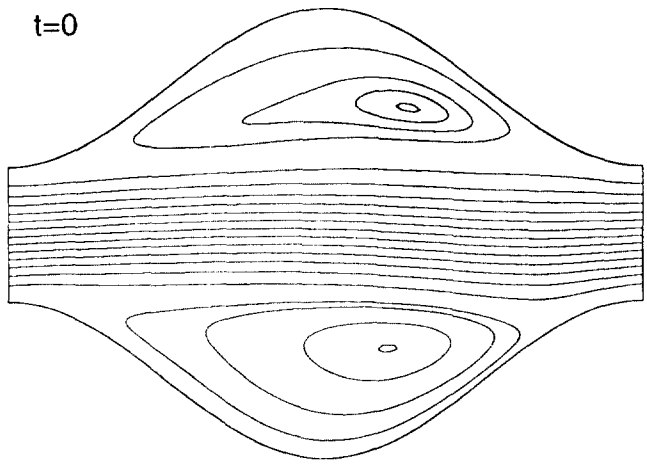

Fig. 4. Unsteady streamlines $\psi(x, y, t)$ at one instant (Re = 100, most unstable mode, $M = 1$ hypothesis).

results (unpublished) show that the TS wavelength takes the value of the geometric period when the relative amplitude E/H_0 of the geometry becomes sufficiently large, i.e. when the wall waviness becomes large enough. It thus seems that there is a critical waviness amplitude E of the geometry beyond which the wavelength of the TS perturbation becomes tuned with the geometric period.

3.3.3. Self-sustained oscillatory flow

Fig. 4 gives as an example the unsteady streamlines at one instant in a period for a Reynolds number of 100 in the case $M = 1$. The results are obtained as shown by Eq. (5) by the superposition of the steady laminar flow and the TS wave. The amplitude ε is chosen sufficiently small to keep the assumption of small perturbation valid (here $\varepsilon = 0.01$). We note the asymmetry of the flow and the behaviour of the unsteady vortex centre, which moves periodically upstream and downstream, with the passage of the TS wave.

Fig. 5 displays the instantaneous wall shear stress coefficient $C_f(x,t)$ defined by

$$C_f(x,t) = \frac{\tau_w(x,t)}{\rho \overline{U}_0^2} \tag{10}$$

at different times during a period. This figure shows that the instantaneous detachment point moves very little around its steady value: $x_d/(2L) = 0.1032 \pm 0.0064$, whereas the reattachment point position has a much larger fluctuation amplitude $x_r/H_0 = 0.837 \pm 0.0294$. These results are qualitatively in good agreement with the flow visualizations made by Nishimura et al. (1986) who writes: "The reattachment point is not fixed but is fluctuating, in contrast to the case of the separation point". This effect is quantified in Table 6 which gives the amplitude of the location fluctuation of the detachment and reattachment points for different amplitudes ε of the flow fluctuations.

It appears that for small fluctuation amplitude ε (less than 10^{-2}), the amplitudes of the oscillations of the detachment and reattachment points follow quasi-linearly the amplitude ε of the flow. When the amplitude increases further (larger than $\varepsilon = 5 \times 10^{-2}$), the amplitude of oscillation of the detachment point increases suddenly, but the validity of this two-dimensional linear stability model is probably then questionable.

Fig. 6 presents the amplitude of the fluctuations of the velocity components ($|u^1|$, $|v^1|$). Large amplitudes are observed in the converging region slightly upstream the reattachment point, where the unsteady boundary layer is redeveloping, in particular around $x/(2L) = 0.8$ as shown by the unsteady wall shear stress coefficient results (Fig. 5).

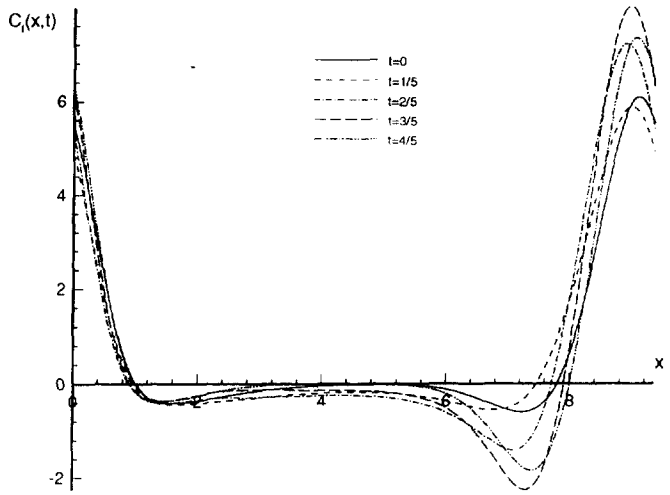

Fig. 5. Local unsteady wall shear stress coefficient $C_f(x, t)$ at different instant.

Table 6

	$\varepsilon = 10^{-4}$	$\varepsilon = 10^{-3}$	$\varepsilon = 10^{-2}$	$\varepsilon = 5 \times 10^{-2}$
$x_{dec}/(2L)$	6.34×10^{-5}	6.34×10^{-4}	6.37×10^{-3}	0.0341
$x_{rec}/(2L)$	2.41×10^{-4}	2.40×10^{-3}	2.94×10^{-2}	0.1812

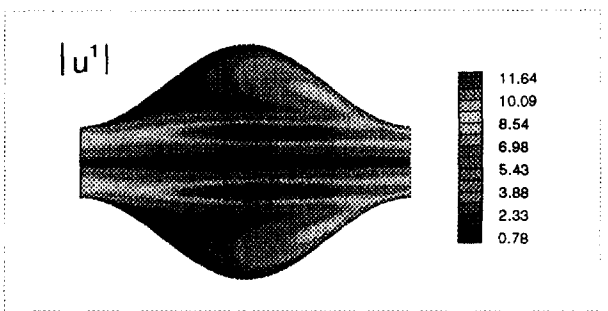

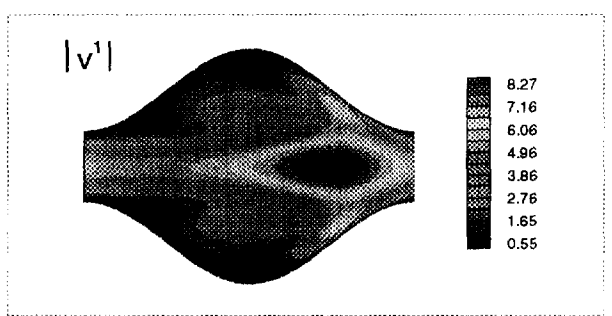

Fig. 6. Velocity amplitude fluctuations components ($|u^1|$, $|v^1|$).

4. Thermal unsteady problem

4.1. The energy equation

To analyse the effects of the TS wave on heat transfer, we consider the unsteady velocity components (u, v) and temperature field T written as

$$u = u^0 + \varepsilon u^1;\ v = v^0 + \varepsilon v^1 \quad \text{and} \quad T = T^0 + \varepsilon T^1. \tag{11}$$

Introducing u, v, T in the unsteady energy equation and keeping first-order terms in ε, the energy equation becomes

$$\frac{\partial T^1}{\partial t} + u^0 \frac{\partial T^1}{\partial x} + v^0 \frac{\partial T^1}{\partial y} - \frac{1}{\mathrm{Pe}} \Delta T^1 = -u^1 \frac{\partial T^0}{\partial x} - v^1 \frac{\partial T^0}{\partial y}. \tag{12}$$

Note that the velocity perturbations (u^1, v^1) introduce in the energy equation a source term whose amplitude is proportional to the amplitude ε of the dynamic perturbation. This source term drives the unsteady temperature perturbation.

4.2. Uniform wall temperature

Under the assumption of a fully developed temperature field and of a uniform and identical (top and bottom) wall temperatures T_w, the unsteady temperature $T(\xi, \eta, t)$ can be written as

$$T(\xi, \eta, t) = T_w - T_r \theta(\xi, \eta, t) \exp(-\tau \xi). \tag{13}$$

The constant τ is the eigenvalue obtained for the steady problem and T_r any reference temperature. The dimensionless unknown temperature field $\theta(\xi, \eta, t)$ is furthermore assumed to be periodic in the ξ direction with the same spatial period as that of the dynamic perturbation (u^1, v^1)

$$\theta(\xi, \eta, t) = \theta^0(\xi, \eta) + \varepsilon \theta^1(\xi, \eta, t). \tag{14}$$

The second member of Eq. (12) is a source term periodic in time with a period defined by the reduced frequency γ_0 of the TS wave.

Using Eq. (14) and with u^1, v^1, θ^1 written as functions: $f_1(\xi, \eta, t) = \mathrm{Real}(\hat{f}(\xi, \eta) \exp(\mathrm{i}\gamma t))$ Eq. (12) becomes

$$-\mathrm{i}\gamma\lambda h^2 \hat{\theta}^1 + \frac{\tau^2}{\lambda\,\mathrm{Pe}} h^2 \hat{\theta}^1 + \tau \left[h \psi_\eta^0 \hat{\theta}^1 + \frac{2h}{\lambda\,\mathrm{Pe}} \left(\eta h' \hat{\theta}_\eta^1 - h \hat{\theta}_\xi^1 \right) \right]$$
$$- h \left(\psi_\eta^0 \hat{\theta}_\xi^1 - \psi_\xi^0 \hat{\theta}_\eta^1 \right) + \frac{1}{\lambda\,\mathrm{Pe}} \Delta \hat{\theta}^1 = -\tau h \hat{\psi}_\eta^1 \theta^0 + h \left(\hat{\psi}_\eta^1 \theta_\xi^0 - \hat{\psi}_\xi^1 \theta_\eta^0 \right). \tag{15}$$

The associated boundary conditions are:

Periodicity: $\hat{\theta}^1(\xi + 2M\pi, \eta) = \hat{\theta}^1(\xi, \eta)$.

Symmetry of the perturbation: $\hat{\theta}^1(\xi, -\eta) = \hat{\theta}^1(\xi, \eta)$.

Constant and uniform wall temperature: $\hat{\theta}^1(\xi, \pm 1) = 0$.

4.3. The numerical method

These periodic and homogeneous boundary conditions allow us to develop the unknown function $\hat{\theta}^1$ as

$$\hat{\theta}^1(\xi,\eta) = \sum_{k=-Nx}^{Nx}\sum_{m=0}^{Ny}\hat{\theta}^1_{k,m}Q_m(\eta)\exp(ik\xi), \tag{16}$$

where Q_m is a polynomial basis, linear combinations of Chebychev polynomials, defined so as to satisfy the homogeneous boundary condition: $\hat{\theta}^1(\xi,\pm1)=0$.

Introducing this development in Eq. (15) and using a spectral Galerkin method, we obtain a full system of linear complex equations which reads

$$\underline{\underline{\hat{\mathbf{A}}}}\,\underline{\hat{\mathbf{X}}} = \underline{\hat{\mathbf{B}}},$$

where $\underline{\hat{\mathbf{X}}}$ is usually the vector of the unknown coefficients $\hat{\theta}^1_{k,m}$.

5. Thermal results

5.1. Nusselt number definition

Earlier work (Blancher, 1991) on steady convective heat transfer analysis has emphasized the importance of using appropriate reference quantities in the definition of the local Nusselt number. Here we choose for reference length the minimum half height of the channel H_0. To get a better knowledge of the influence of the TS wave on convective heat transfer we must take into account the dynamic unsteady effect. For this reason, the local and instantaneous Nusselt number is defined as the ratio of the local and instantaneous heat flux density $\varphi(x,t)$ versus the difference between the constant wall temperature T_w and the time average bulk temperature $\langle\overline{T}_b(x)\rangle$ in each section x,

$$\mathrm{Nu}(x,t) = \frac{\varphi(x,t)}{\langle T_w - \overline{T}_b(x)\rangle}, \tag{17}$$

where $\varphi(x,t) = (\partial T/\partial\eta)_w = \varphi^0(x) + \varepsilon\varphi^1(x,t)$ is the reduced heat flux density. The bulk temperature is

$$\langle\overline{T}_b(x)\rangle = \int_0^1 \langle uT\rangle\,\mathrm{d}\eta, \quad \text{and thus} \quad \langle T_w - \overline{T}_b(x)\rangle = \int_0^1 \langle\hat{\psi}\hat{\theta}_\eta\rangle\,\mathrm{d}\eta. \tag{18}$$

Introducing the corresponding expressions this average temperature difference becomes

$$\langle T_w - \overline{T}_b(x)\rangle = \int_0^1 \psi^0\theta^0_\eta\,\mathrm{d}\eta + \varepsilon^2\int_0^1 \Big(\mathrm{Re}(\hat{\psi}^1)\mathrm{Re}(\hat{\theta}^1_\eta) + \mathrm{Im}(\hat{\psi}^1)\mathrm{Im}(\hat{\theta}^1_\eta)\Big)\,\mathrm{d}\eta \tag{19}$$

and thus

$$\langle T_w - \overline{T}_b(x)\rangle = \Delta T^0(x) + \varepsilon^2\Delta T^1(x). \tag{20}$$

Under the assumption of small amplitude, the unsteady Nusselt number can thus be written as

$$\mathrm{Nu}(x,t) = \frac{\varphi^0(x) + \varepsilon\varphi^1(x,t)}{\Delta T^0(x) + \varepsilon^2\Delta T^1(x)}. \tag{21}$$

The effect of the TS wave on the convective heat transfer thus appears through two parameters:
- the amplitude of the unsteady heat flux density $|\varphi^1(x,t)|$,
- the reference temperature perturbation $\Delta T^1(x)$.

5.2. Straight channel

Although it is well known that the transition from laminar to turbulent flow in a straight channel is not triggered by TS waves (Orszag and Patera, 1983), it seems interesting to investigate the effect of a TS wave on the convective heat transfer in view of further comparison. Introducing this two-dimensional perturbation in the unsteady energy equation and after linearization, we obtain the total unsteady temperature field $T(x,y,t)$ shown at one instant in Fig. 7. The thermal perturbation associated with the dynamic TS wave disturbs the thermal boundary layer periodically in time and space giving a higher fluctuation of the heat flux density in the vicinity of the wall. This perturbation leads to a modification of the convective heat transfer as shown in Table 7 which gives the heat flux density amplitude $|\varphi^1|$ and the temperature difference modification $\varepsilon^2\Delta T^1$ ($\varepsilon=0.01$) for different Prandtl numbers.

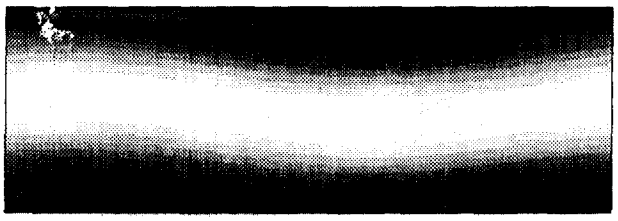

Fig. 7. Straight channel – unsteady isotherms $T^{0,S}(x,y,t)$ at one instant.

These values should be compared with the steady values: $\varphi^{0,S}=3.128$ and $\Delta T^{0,S}=1.659$, which are independent of the Prandtl number and give the classical Nusselt number $\mathrm{Nu}^{0,S}=\varphi^{0,S}/\Delta T^{0,S}=1.8854$ with our Nusselt number definition. It thus appears that the TS wave has a large influence on the heat flux density amplitude but affects very little the bulk temperature. It is furthermore noted that the Prandtl number has an important effect on the heat flux density amplitude whereas it has very little effect on the bulk temperature.

5.3. Wavy channel

In this part, we consider the geometry defined by its periodicity length $2L=8H_0$ and amplitude $E=2H_0$ which is exactly that considered by Sobey, slightly different from Nishimura's. All the results are obtained in the case $M=1$ and development orders identical to those used for the dynamic study: $Nx=8$ and $Ny=32$.

5.3.1. Steady results

As an example Fig. 8 presents the steady isotherms $T^0(x,y)$ for the fully developed flow ($\mathrm{Re}=100$ and $\mathrm{Pr}=1$). Fig. 9 shows the local variation of the heat flux density $\varphi^0(x)$ at the wall and the reference temperature difference ΔT^0 for the steady solution. It is noted that the local steady Nusselt number variation comes principally from the variation of the heat flux density since the bulk temperature remains approximately constant. We have shown that local enhancements up to 80% are obtained slightly downstream of the reattachment point by comparison with the results for a straight channel: $\varphi^{0,S}=3.128$ and $\Delta T^{0,S}=1.659$.

5.3.2. Unsteady results

To visualise the effect of the TS wave on the temperature field, Fig. 10 presents the unsteady isotherms $T(x,y,t)$ at

Table 7

Pr	$\lvert\varphi^1\rvert$	$\varepsilon^2\Delta T^1$
0.1	1.61	-1.21×10^{-3}
1	4.82	-1.21×10^{-3}
10	13.82	-1.15×10^{-3}
100	54.6	-1.28×10^{-3}

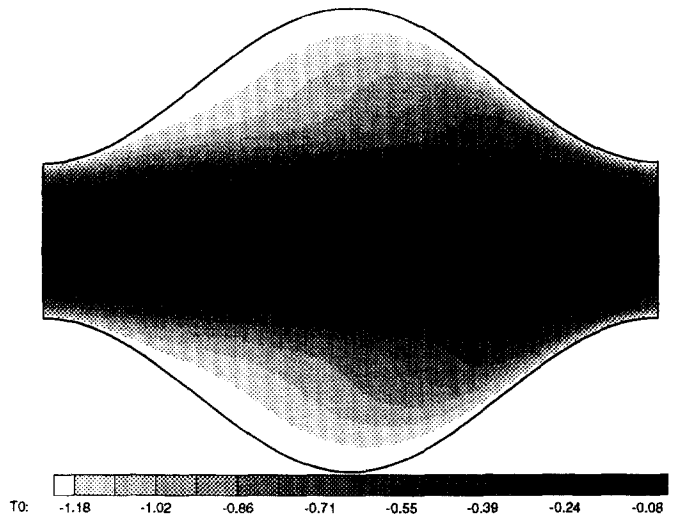

Fig. 8. Wavy channel – Steady isotherms $T^0(x,y)$ (Re = 100; Pr = 1).

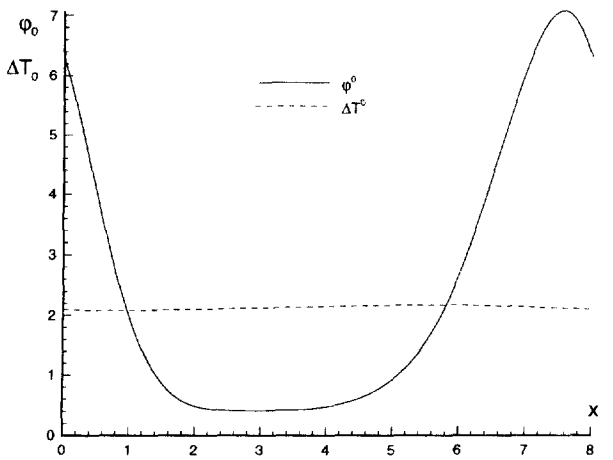

Fig. 9. Heat flux density and temperature reference – steady flow (Re = 100, Pr = 1).

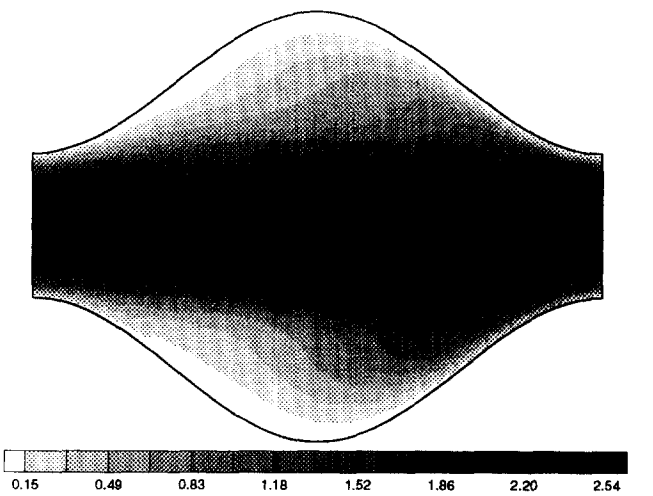

Fig. 10. Unsteady isotherms $T^0(x, y, t)$ at one instant.

one time within a period. We can see how the thermal boundary layer is affected by the TS wave, particularly in the converging region where the dynamic boundary layer is strongly perturbed.

Fig. 12 presents the amplitude of the fluctuation $|\theta^1|$ for Re = 100 and Pr = 1. We observe that the large amplitude fluctuations are located in the boundary layer near the reattachment point. This region corresponds to the maximum amplitude $|u^1|$ and $|v^1|$ as shown in Fig. 6. These velocity fluctuations and temperature perturbations associated with large vorticity gradients, induce a strong local heat transfer modification between the wall and the fluid, for this particular case of constant wall temperature.

To analyse the effect of this perturbation on the heat transfer, we present in Fig. 11 the heat flux density perturbation $|\varphi^1|$ and the difference temperature perturbation $\varepsilon^2\Delta T^1$ as a function of x. We note two maximums of heat flux density amplitude, localised around the steady detachment and reattachment points. Moreover a small variation of the temperature reference is visible slightly upstream the reattachment point. As expected the large heat flux amplitudes are correlated with position of maximum velocity, temperature and vorticity amplitude around the reattachment point, where the wall shear

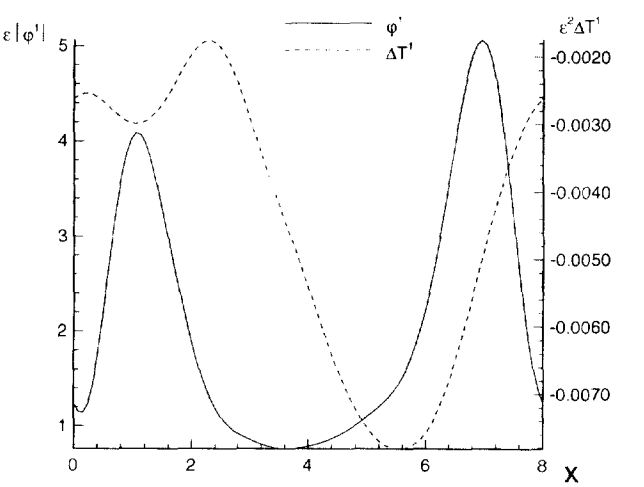

Fig. 11. Heat flux density and temperature reference amplitudes – unsteady flow (Re = 100, Pr = 1).

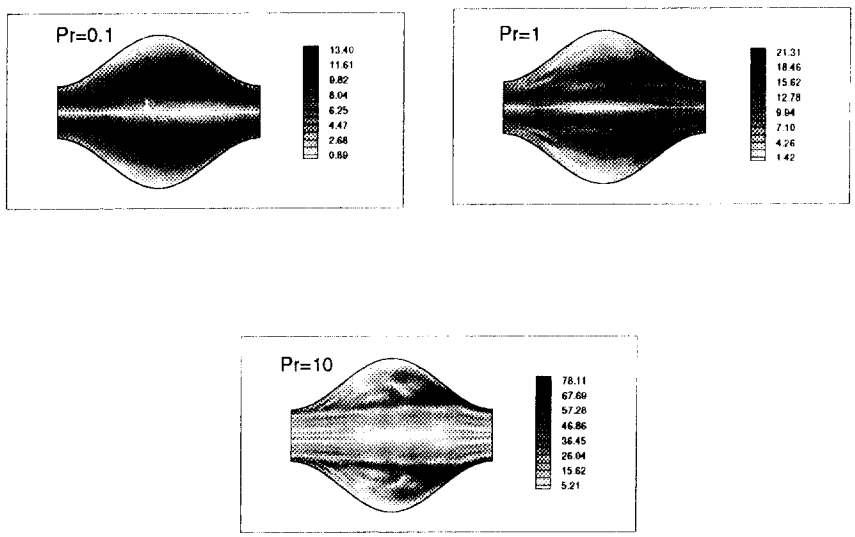

Fig. 12. Temperature amplitude fluctuation $|\theta^1(x,y)|$.

stress amplitude is maximum. This qualitative result agrees with similar studies on the local heat transfer in a sudden expansion by Sparrow et al. (1987).

5.3.3. Reynolds number effect

The above results have been obtained for a Reynolds number equal to 100 and an amplitude fluctuation set to $\varepsilon = 0.01$. We have noted that a pair of complex eigenvalues crosses the Reynolds axis (Fig. 2), which corresponds to a Hopf bifurcation. Non-linear time integrations have indicated that this bifurcation is of supercritical type as shown by Guzman and Amon (1993). Consequently, following Landau's theory (Landau and Lifshitz, 1971), for Reynolds numbers sufficiently close to the critical Reynolds number, all quantities are thus expected to vary sinusoidally in time with an amplitude ε proportional to

$$\varepsilon = A(\mathrm{Re} - \mathrm{Re}_c)^{1/2} \tag{22}$$

and consequently, in the linear approximation used here, average effects in time should remain identically zero. However, the non-linear term $\langle uT \rangle$ which appears in the definition of the conventional bulk temperature results in a non-zero time averaged second-order ε^2 effect in the time averaged temperature difference which reads

$$\langle T_w - \overline{T}_b(x) \rangle = \Delta T^0 + (\mathrm{Re} - \mathrm{Re}_c)\Delta T^1.$$

The unsteady Nusselt number reads then

$$\mathrm{Nu}(x,t) \approx \mathrm{Nu}^0 \left(1 + (\mathrm{Re} - \mathrm{Re}_c)^{1/2} \frac{|\varphi^1|}{\varphi^0} \sin(\gamma t + \vartheta)\right) \times \left(1 - (\mathrm{Re} - \mathrm{Re}_c)\frac{\Delta T^1}{\Delta T^0}\right), \tag{23}$$

where the first term in brackets on the right-hand side varies sinusoidally in time while the second is constant. Its time averaged value reads, to the first order in $(\mathrm{Re} - \mathrm{Re}_c)$:

$$\mathrm{Nu}(x) \approx \mathrm{Nu}^0 \left(1 - (\mathrm{Re} - \mathrm{Re}_c)\frac{\Delta T^1}{\Delta T^0}\right) \tag{24}$$

and thus shows a small but non-zero second-order augmentation, since ΔT^1 is negative. This effect increases significantly with increasing Prandtl number.

5.3.4. Prandtl number effect

To illustrate Prandtl number effects, Fig. 12 presents the temperature perturbation amplitude for different Prandtl numbers 0.1, 1 and 10 (the Reynolds number is kept equal to 100). It is seen that increasing the Prandtl number deeply affects the thermal boundary layer especially in the converging section of the flow. In addition, Fig. 13 presents the evolution of the heat flux density amplitude fluctuation for these different Prandtl numbers with the same TS amplitude. As for a straight channel, we observe the strong influence of the Prandtl number on the heat flux density amplitude particularly at the detachment and reattachment points.

6. Conclusion

We have numerically obtained the unsteady temperature field for an unsteady self-sustained laminar flow in a channel of periodic cross section. The perturbation driven by a TS wave induces strong amplitude fluctuations of velocities, vorticity and temperature in the reattachment region of the boundary layer in the converging section. These fluctuations lead to very large amplitude of the heat flux density, these amplitude increasing strongly with the Prandtl number near the reattachment point. With the hypothesis of small amplitudes perturbation ($\varepsilon < 0.01$), the mean wall to bulk temperature difference is only slightly modified by the TS wave and the

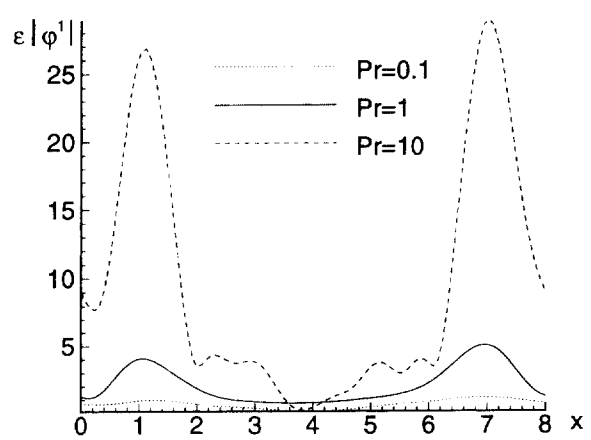

Fig. 13. Heat flux density amplitude $|\varphi^1(x,y)|$.

effect of the TS wave on the average heat transfer remains small but non-zero even in the framework of a linear approximation.

Acknowledgements

This work was supported by C.N.U.S.C. through a computing grant for the use of the parallel SP2 computer.

References

Asako, Y., Faghri, M., 1987. Finite volume solutions for laminar flow and heat transfer in a corrugated duct. J. Heat Transfer 109, 627–634.

Blancher, S., 1991. Transfert convectif stationnaire et stabilite hydrodynamique en géométrie périodique, Thèse de Doctorat, Université de Pau.

Blancher, S., Creff, R., Batina, J., Andre, P., 1992. Transferts thermiques et stabilité hydrodynamique en géométrie périodique. Proceedings colloque SFT, Sofia Antipolis.

Blancher, S., Creff, R., Batina, J., Andre, P., 1994. Hydrodynamic stability in periodic geometry. Finite Elements in Analysis and Design 16, 261–270.

Canuto, C., Hussaini, M.Y., Quarteroni, A., Zang, T.A., 1988. Spectral Methods in Fluid Dynamics. Springer, New York.

Drazin, P.G., Reid, W.H., 1981. Hydrodynamic stability. Cambridge University Press, Cambridge.

Ellouze A., 1993. Simulation de la dynamique d'un écoulement en canal ondulé, étude du transfert convectif associé. Thèse de Doctorat, Pau.

Ghaddar, N.K., Korczak, K.Z., Mikic, B.B., Patera, A.T., 1986. Numerical investigation of incompressible flow in grooved channels – Part 1: Stability and self sustained oscillations. J. Fluid Mech. 163, 99–127.

Greiner, M., Chen, R.F., Wirtz, R.A., 1990. Heat transfer augmentation through wall shape induced flow destabilisation. J. Heat Transfer 112, 337–341.

Guzman, A.M., Amon, C.H., 1993. Flow patterns and force convective heat transfer in converging–diverging channel. Trans. ASME 237, 43–53.

Landau, L.D., Lifshitz, 1971. Mécanique des fluides. Editions Mir, Moscou.

Nishimura, T., Ohori, Y., Kawamura, Y., 1983. Flow characteristics in a channel with symmetric wavy wall for steady flow. J. Chem. Eng. Japan 17 (5), 466–471.

Nishimura, T., Ohori, Y., Kajimoto, Y., Kawamura, Y., 1985. Mass transfer characteristics in a channel with symmetric wavy wall for steady flow. J. Chem. Eng. Japan 18 (6), 550–555.

Nishimura, T., Kajimoto, Y., Tarumoto, A., Kawamura, Y., 1986. Flow structure and mass transfer for a wavy wall in transitional flow regime. J. Chem. Eng. Japan 19 (5), 449–455.

Nishimura, T., Murakami, S., Arakawa, S., Kawamura, Y., 1990. Flow observations and mass transfer characteristics in symmetrical wavy-walled channels at moderate Reynolds number for steady flow. Int. J. Heat Mass Transfer 33 (5), 835–845.

Orszag, S.A., 1971. Accurate solution of the Orr Sommerfeld stability equation. J. Fluid Mech. 50, 689 703.

Orszag, S.A., Patera, A.T., 1983. Secondary instability of wall-bounded shear flows. J. Fluid Mech. 128, 347–385.

Sobey, I.J., 1980. On flow through furrowed channels – Part 1: Calculated flow patterns. J. Fluid Mech. 96, 1–26.

Sparrow, E.M., Kang, S.S., Chuck, W., 1987. Relation between the points of flow reattachment and maximum heat transfer for regions of flow separation. Int. J. Heat Mass Transfer 30 (7), 1237–1246.

Stephanoff, K.D., Sobey, I.J., Bellhouse, B.J., 1980. On flow through furrowed channels, Part 2: Observed flow patterns. J. Fluid Mech. 96, 27–32.

Stephanoff, K.D., 1980. Self-excited shear layer oscillations in a multi-cavity channel with a steady mean velocity. J. Fluids Engineering 108, 338–342.